

MECHANISM OF BOULDER TRANSPORT DURING EXTREME WAVE EVENTS ALONG THE EASTERN FLANK OF THE ARABIAN SEA

Afzal Khan^{a,b*}, Avichal Singh^a, Mahendrasinh S Gadhavi^c, Javed N Malik^a

^aDepartment of Earth Sciences, Indian Institute of Technology Kanpur, 208016, Uttar Pradesh, India

^bSchool of Civil Engineering and Architecture, Adama Science and Technology University, Adama, 1888, Oromia, Ethiopia

^cDepartment of Civil Engineering, L. D. College of Engineering, Ahmedabad, 380015, Gujarat, India

Article history

Received

07 April 2021

Received in revised form

15 July 2021

Accepted

29 July 2021

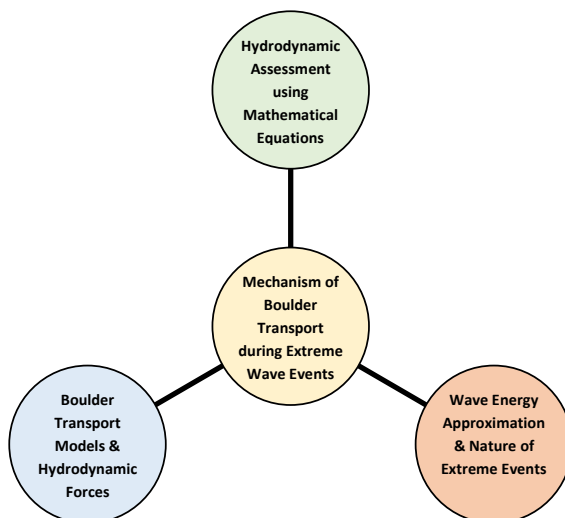
Published online

31 August 2022

*Corresponding author

afzal@iitk.ac.in

Graphical abstract



Abstract

The study presents hydrodynamic mechanism of boulder transportation along the rocky coastal margins with a case study from the eastern flank of the Arabian Sea. Limestone blocks ranging in size from small (1.3, 0.95, 0.35) m to large (2.9, 1.68, 0.5)m scattered over a rocky platform were considered for the approximation of wave energy. The boulders with prominent imbrications indicative of flow direction were used to assess the minimum flow velocity to initiate boulder transport during extreme wave events. The irregular /polyhedral boulders, previously a part of sub-aerially exposed jointed limestone strata, were detached and transported from the rocky coastal platform under the impact of high energy waves. We calculated velocity and height for dynamic waves required to transport boulders onshore using boulder dimensions i.e., length (a-axis), width (b-axis), and height (c-axis). By applying hydrodynamic equations, it is deduced that the average wave velocity required to transport boulders of such dimensions onshore must be $\geq 7.28\text{m/s}$ and the corresponding average wave heights must be $\geq 5.51\text{m}$ and $\geq 1.38\text{m}$ in case of the storm and tsunami events respectively. Based on largest clast recorded, $\approx 7\text{m}$ high storm waves and $\approx 2\text{m}$ high tsunami waves are capable of transporting $\approx 2.5\text{m}^3$ tabular boulders along rocky coastal margins. Since this region has documented records of very-severe cyclonic storms affecting the coastal landscape in addition to the widespread impact of 1945 tsunami, we suggest that boulders deposition on the eastern flank had received inputs from storm as well as tsunami events for the last few decades.

Keywords: Arabian Sea, Extreme wave events, Hydrodynamic mechanism, High-energy waves, Imbricated boulders

© 2022 Penerbit UTM Press. All rights reserved

1.0 INTRODUCTION

Transported boulders have been used as indicators of high energy waves in numerous studies, but direct observations of boulders transportation due to known extreme wave events are relatively rare [5-9, 15-20, 35-38]. The transport ability of storms and tsunami waves is well studied by comparing the images/photographs of the coastal platform before and after

impacts [5-9, 15-20, 31-38]. The documented boulder transport by the 2004 Indian Ocean tsunami and tropical storms in the Pacific Ocean witnessed the extent of inundation and wave energy [7, 8, 31-38]. Storms are capable of quarrying large boulders from the shoreline but do not usually have sufficient energy to displace them far inland [5, 8, 9, 35-38]. By contrast, the long wave of tsunamis is more likely to transport megaclasts inland due to the longer duration of their action [7, 9, 20,

31-34]. Makran subduction zone is generated by the convergence between the Eurasian and the Arabian Plates which constitutes one of the largest accretionary wedges on the planet [29, 40]. The zone constitutes a shallow subduction angle with a high sediment input of 7km and therefore it is seismically active [29]. Several scientists have studied historical seismic events in the Makran subduction zone, and presented a preliminary estimation of tsunami hazard along the encircling coastlines [3, 4, 10-13, 20-24, 29, 30, 39].

In this study, we explored a segment of eastern coastline of the Arabian Sea which is indirectly associated with Makran subduction zone. This region falls under the risk zone of tsunamigenic earthquakes originated from the Makran subduction zone (Figure 1). The eastern coastline has also witnessed cyclonic storms of severe to very severe category in the past; some of them caused extensive devastation along the Saurashtra coast [25-28]. The Arabian Sea is known to generate storms of high intensity every 2 to 3 years [25-28]. The chain of piled, scattered, and imbricated boulders running along the surveyed coastline might have been deposited by any one or more of the aforementioned event/s. In this paper, an attempt has been made to understand hydrodynamic mechanism behind transportation of the tabular boulders along rocky coasts and to determine the nature of causative event/s. Geometry of boulder size and fluid flow dynamics are taken into account to estimate the potential size of the waves required for transportation of such boulders.

2.0 TECTONIC SETTING AND COASTAL GEOMORPHOLOGY

Makran is a part of the coastal territory of Iran and Pakistan stretching over the Strait of Hormoz, in the south of Iran, to Karachi-Pakistan and surrounded by Arabian Plate on its south-west and Indian Plate on its south-east direction [10, 11, 21, 39]. The Makran coast is part of the accretionary wedge of the MSZ formed by the subduction of the Arabian plate under the Eurasian plate [3, 23, 29]. The convergence rate along the subduction zone varies between 2.3 cm/yr in the western end and 2.9 cm/yr along the eastern margin [23, 29]. The region associated with MSZ and Murray Ridge has experienced tsunamigenic earthquakes in the past, where 326BC and 1945 tsunamis have documented records of impacting the Saurashtra coast (Fig. 1). However, the study segment has not only been affected by tsunami waves but also by storm waves, where 1975, 1982, 1998, 2001, and 2007 cyclonic storms have recorded their tracks with close encounters (Fig. 1). The NW-SE alignment of the coastline is vulnerable to tsunamis/storms based on their sources in the Arabian Sea.

The western coastline of the Arabian Sea extensively shows hard rocks and deserts in the form of bays, cliffs, high-raised sandy platforms with gentle slopes [10, 20]. The northern belt is dominated by rocky and sandy deserts with steep slopes directing towards the Arabian Sea [20-23]. The eastern coastline shows distinct regime of geomorphology and sedimentology probably due to its bathymetry, coastal configurations (land contours), hydrodynamic setting, and arid climate (Figure 1). Moving from land to seaward, this coastline shows extensive stretch of terraces, eolian dunes, sandy cliffs, boulder deposits, and rocky tracts running parallelly along the shoreline (Figures 2, 3). The boulder deposits exhibit

imbrications with stacking and piling patterns due to certain hydrodynamic processes associated with extreme wave events along the eastern coastline (Figures 2, 3). Our study focuses on this hydrodynamic mechanism of transporting such boulders onshore.

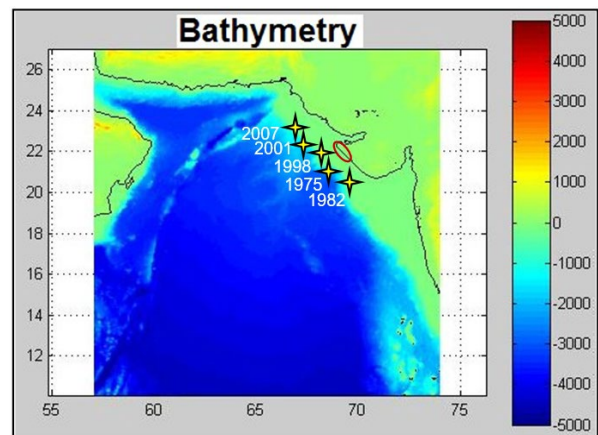
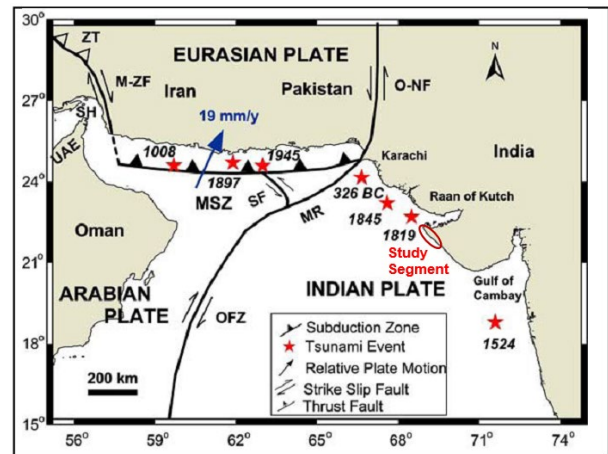


Figure 1 Map showing tectonic features and tsunamigenic earthquakes associated with the Arabian Sea [10]. Tsunamis and storms proximity are marked by the red and yellow stars respectively. The study segment on the Saurashtra coast is marked by the red oval circle. Major tectonic features are Makran Subduction Zone (MSZ), Murray Ridge (MR), Owen Fracture Zone (OFZ); Second Map shows the bathymetry of the Arabian Sea [10, 11, 29].

3.0 STUDY AREA

The study area is located along the eastern flank of the Arabian Sea, which covers a segment of the Saurashtra coast of India (Fig. 1). We surveyed multiple locations along the study segment bounded within the coordinates 21.9923° and 22.4796°, 69.1856° and 69.0676° along the Saurashtra coast of India (Fig. 1). The region is bordered by a windy coast controlling its onshore depositional environment which has formed eolian dunes running parallel to shoreline, and therefore, it is a wave-dominated coast (Figs. 2, 3). Though this region has experienced many near/far source earthquakes in the past, this study is restricted to tsunamigenic earthquakes. Most of known tsunamis impacted with low intensity except the 1945 which caused widespread devastation due its high wave energy [11-

13, 22]. The region is marked by a shallow continental shelf (as shown in Figure 1: bathymetry map), large-scale geomorphic divisions (i.e., Rann of Kutch, gulf), and tectonic elements (i.e., subduction, faults). In this segment of the coast, rock formations are mainly made up of limestone along with small and irregular horizons of sand-clay members (Figure 3).



Figure 2 Southward facing photo shows boulders that are extensively scattered along the shoreline manifesting the gentle topographic slope. The boulders are blanketed over rocky tract with imbrications indicating flow-directions within a 20-25m wide fringing zone associated with the shoreline.

In this region, limestone is observed as the topmost lithological unit with the underlying sandstone and irregular sand-clay units forming a rocky coastal platform (Figure 3). The topmost limestone unit shows joint sets striking N30°W to N35°W (Figs. 3-5). Due to solution activity and presence of joint sets, limestone had been no longer remained stable and fractured along the weakened zone (Figures 4, 5). This process leads to transformation of rocky platform into fragmented tabular boulders, which is accompanied by detachment and transportation of boulders under the wave activity (Figures 2-5).

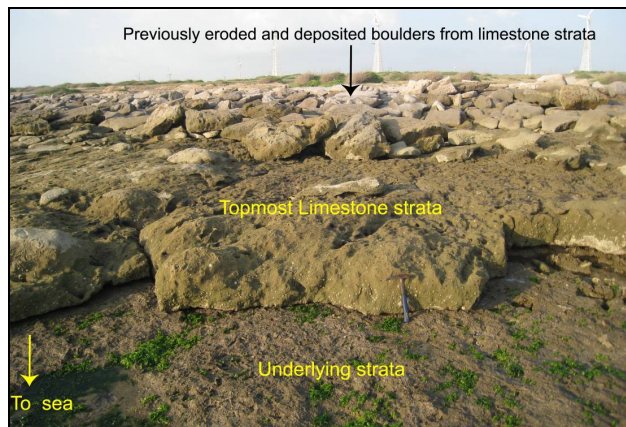


Figure 3 Landward facing photo shows stratified layers of sandstone (lowest), limestone (middle), and boulder deposits (top). We observed that mostly limestone layer is removed and transported due to its soft nature and weak tendency against wave action, whereas sandstone mostly remained stable due to its resistive nature and found unevenly eroded.

4.0 METHODOLOGY AND BOULDER TRANSPORT MODELS

During the survey we measured long (a), intermediate (b), and short (c) axes of several boulders deposited above mean sea level along with the directions of imbrications. To normalize the irregularities in the shape of boulders the mean length of axes was considered. The unit mass of the limestone boulders was determined using the volumetric method as $2.7 \times 10^3 \text{ kg/m}^3$ for all boulders, and using density their weight is estimated. By applying hydrodynamic equations using boulder parameters, we calculated velocity and height for dynamic waves (storm/tsunami) required to transport boulders onshore.

Here we attempt to generalize hydrodynamic mechanism of boulder transport with the help of schematic models which explain the process of boulders deposition during the extreme wave events (Figures 5-8). It is well known that the pattern of imbrications is specifically associated with the high energy waves, i.e., tsunami, storm [5, 7-9, 31-38].

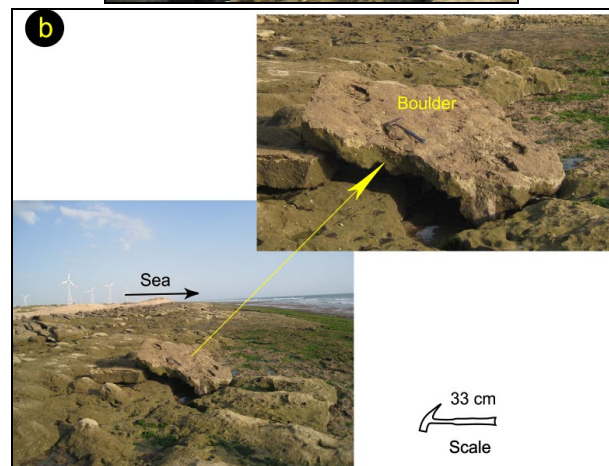
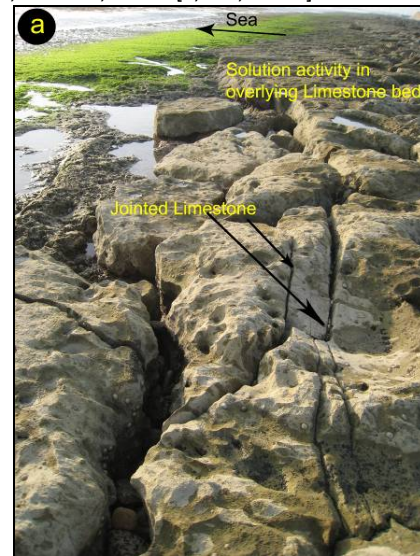


Figure 4 (a) Northward facing photo shows jointed and fractured limestone strata marked by intense solution activity. The solution cavities and structures are clearly visible over the fragmented limestone strata. (b) Southward facing photo showing the rocky coastal tract overlain by large boulders. The inset image of the large boulder gives idea of its dimension with the measurement of hammer length.

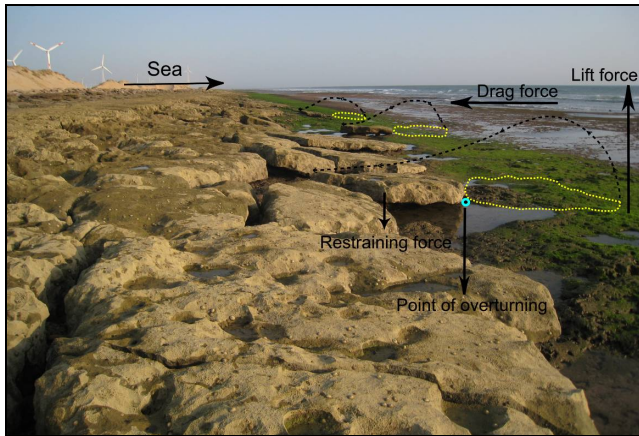


Figure 5 Southward facing photo shows linear dune ridge on the left, limestone platform in the middle, and sea on the right. The dissolution structures are clearly visible on the eroded and fractured limestone bed where it has transformed into tabular boulder fragments. The hydrodynamic mechanism of transportation is illustrated by pointing drag, lift, and restraining forces applied on a boulder due to action of high energy waves. The yellow dashed-line features the previous locations of respective boulders before overturning.

We observed prominent imbrications of boulders all along the surveyed coastline which indicates their deposition is linked to high-energy waves (Figures 2, 3). We elucidate the force components related to high-energy waves causative of erosion, transportation and deposition over the rocky tract topography existed during extreme wave events (Figures 5-8).

5.0 HYDRODYNAMIC ASSESSMENT RESULTS

The hydrodynamic equations related to boulder transport models have been discussed in several studies [1, 6, 14, 17-19, 31]. Initially, Nott developed hydrodynamic equations to calculate the minimum wave height capable of initiating boulder movement [17, 18]. These equations involve the boulder's dimensions, including the long, intermediate, and short axes, boulder and water density, coefficient of drag, coefficient of lift, coefficient of mass, gravitational constant and instantaneous flow acceleration [18]. Nott's equations consider three possible pre-transport settings: submerged, subaerial and joint-bounded [17, 18]. In this study the surveyed boulders are typically sub-aerially exposed (Figures 2-5). Simplified boulder transport equations (1 & 2) for tsunami and storm waves respectively under this setting are as follows [17, 18]:

SUBAERIAL BOULDER PRE-SETTING

$$H_t \geq [0.25(\rho_s - \rho_w / \rho_w) \{ (2a - C_m(a/b)) (\ddot{u}/g) \}] / [C_D(ac/b^2) + C_L] \quad (1)$$

$$H_s \geq [(\rho_s - \rho_w / \rho_w) \{ (2a - 4C_m(a/b)) (\ddot{u}/g) \}] / [C_D(ac/b^2) + C_L] \quad (2)$$

According to Nott's equations, the capability of transporting boulders of tsunami waves is fourfold as compared to storm waves, due to their longer wave period. Storms dissipate their energy during landfall and only cause marginal deposition. Wave transport capacities are also strongly influenced by the boulder shape. For instance, the higher wave height is required

to transport angular shaped boulders than spherical boulders, similarly greater height necessitates transporting planar rectangular boulders [1, 6, 18, 19]. However, later it was pointed out that Nott's equations yield exaggerated wave heights. Moreover, here the length of the lever arm and acceleration of the water around subaerial boulders are also not considered [1]. Under modified conditions, the coefficient of lift is 1 for the cuboid, whereas 2 for the prismatic boulders. Hence, it is suggested that the following corrections must be applied to the subaerial boulder transport equations [1]:

$$H_t \geq [0.5bc(\rho_s - \rho_w) / \rho_w - \rho_s C_m \ddot{u} / (pwg)] / [C_D c^2 + C_L b^2] \quad (3)$$

$$H_s \geq [2bc(\rho_s - \rho_w) / \rho_w - \rho_s C_m \ddot{u} / (pwg)] / [C_D c^2 + C_L b^2] \quad (4)$$

Where H_t is the tsunami wave height and H_s is the storm wave height at breaking point. a , b and c are the boulder axes lengths; ρ_w is the sea water density; ρ_s is the boulder's density; C_D is the coefficient of drag = 1.2; C_L is the coefficient of lift = 0.15; C_m is the coefficient of mass = 1; whereas \ddot{u} is the flow acceleration = 1 m/s^2 ; and g is the gravitational acceleration = 9.81 m/s^2 .

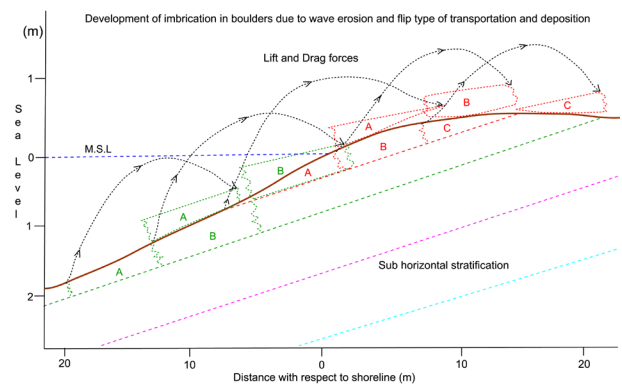


Figure 6 Schematic model illustrates the mechanism of boulder transportation from the stratified layers of limestone. The boulders A, B, C were detached, transported and settled over the topography after few overturning actions as shown by the arrows. The model shows how the morphology of topography changes through time.

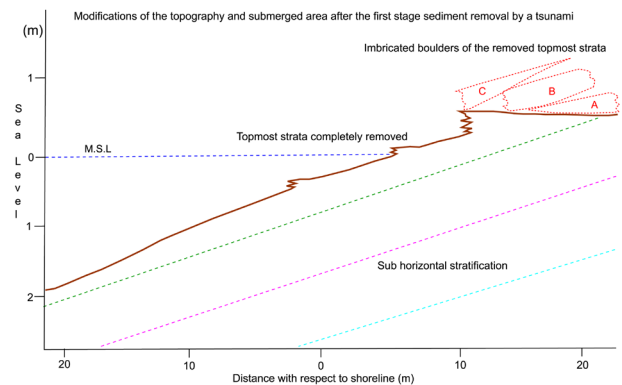


Figure 7 Schematic model illustrates next stage settling of the boulders from the top layer of limestone. The boulders A, B, C were flipped, rearranged and re-settled forming imbrications pattern over the topography. The model shows how the morphology (surface and slope) of topography (marked in brown) is modified through time.

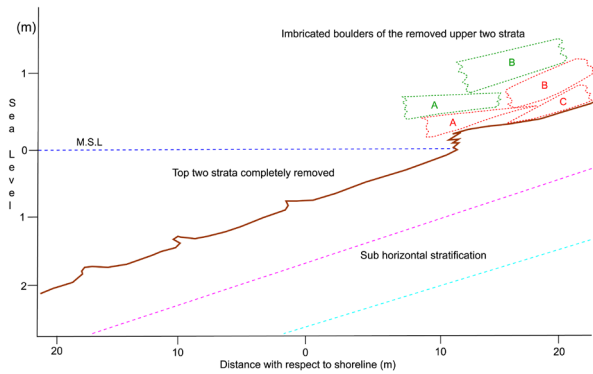


Figure 8 Schematic model illustrates the final stage settling of the boulders over the topographic surface from the two (red and green) stratified layers of limestone. The boulders A, B, C were transported, re-arranged through flipping and re-settled forming imbrications pattern over the topography. The model shows how the morphology (surface and slope) of topography (marked in brown) is modified through time. Blue line marks the Mean Sea Level (MSL).

In some of the works on boulders, coefficient of lift has been taken as 0.178, but it is not reasonable since every value between 0.05 and 0.2 is possible [1, 6]. In nature, boulders are rarely square stones with rectangular flat sides, the value of coefficient of drag can be more accurately implied within a range of 0.8 to 1.2 [1-3, 6, 14]. Since we have also observed some jointed limestone platforms in the field; therefore, we further applied following equations for Joint-bound boulder pre-setting [1]:

$$Ht \geq [0.5c(\rho_s - \rho_w) / \rho_w] / C_L \quad (5)$$

$$Hs \geq [2c(\rho_s - \rho_w) / \rho_w] / C_L \quad (6)$$

Therefore, under specific conditions we adopted the improved model of equations (3-6) for the calculation of wave velocity and wave height required to transport such boulders in case of tsunami and storm events respectively [1-3, 6, 14]. This mathematical approach can be applied on boulders under different conditions, such as they may be dislocated from a cliff or a submerged or sub-aerially exposed jointed rocky platform by the action of storm or tsunami waves [5, 6, 14, 19]. Since jointed limestone platform is not a uniform case in study, Table 2 is not considered for the approximation of wave energy.

6.0 RESULTS

We selected fifteen locations along the study segment and picked up the largest boulders from each site (i.e., B1 to B15) for assessing the minimum wave energy required for their displacement. Based on the wave energy (i.e., flow velocity, wave height), depositional pattern, inundation extent, and boulder size/shape, we deduced information about the nature of extreme wave event/s. We used dimensions of the boulders, i.e., length (a-axis), width (b-axis) and height (c-axis), as well as component of the forces applied during the time when a wave hits a submerged or sub-aerially exposed boulder over the rocky platform (Figures 2-5). Boulder dimensions measured in field from the selected sites along the coastline are given in the Tables 1-2. The largest boulder identified out of all the locations was measured as 2.62x1.98x0.48 (a, b, c) in meters of

dimensions. The hydrodynamic assessment in this study is based on the assumption that the speed of the current remains constant for all extreme wave events.

By applying hydrodynamic equations with the measured data, the calculation shows that the wave velocity required for initiating boulder transport by any high-energy event ranges from 4.98 to 8.35m/s, where the corresponding required wave height ranges from 0.63 to 1.78m for tsunami and from 2.53 to 7.11m for storm. Based on the largest boulder identified from the study segment, the results suggest that with the uniform velocity ≈ 7 m high storm waves and ≈ 2 m high tsunami waves are required to transport ≈ 2.5 m³ tabular boulders along rocky coastal margins (Table 1).

In this exercise, consideration must be given to the fact that the maximum size of boulders moved onshore does not necessarily represent the maximum transport capacity of a storm wave or a tsunami flow, but may only be indicative of the maximum size of available clasts. Therefore, even a field of large boulders located onshore may only give an approximation of minimum wave or flow energy [14]. Considering this fact, we plumped for the averaged wave parameters for the approximation of wave energy. According to our results, the average wave velocity for a tsunami/storm required to transport boulders onshore of such dimensions must be ≥ 7.28 m/s and the corresponding average wave heights must be ≥ 5.51 m and ≥ 1.38 m in case of the storm and tsunami events respectively (Table 1).

7.0 CONCLUSION AND DISCUSSION

We carried out hydrodynamic evaluation of the boulder transport along the selected segment on eastern flank of the Arabian Sea in order to understand nature of the causative extreme wave events. Tsunami and storm exhibit different hydrodynamic characteristics and therefore strike a coastline with their specific wave patterns and sediment transport mechanism. Onshore boulder deposits along a coastline, which is vulnerable to tsunamis as well as cyclonic storms, can't be linked to a specific extreme-wave event unless detailed observations are carried out. Estimating wave parameters by applying hydrodynamic equations on deposited clasts is one way of understanding the nature of events. Our study reveals the characteristics of events responsible for boulders transport and deposition along the studied transect, which is very important to understand the wave dynamics of the coastline. Previous studies have linked these boulder deposits to tsunamis; however, our study provides evidence that the past storms along this coastline were also capable of transporting and depositing such boulders onshore.

The study segment has pre-survey documented records of very severe cyclonic storms like 1975, 1982, 1998, 2001, and 2007 which impacted this coast with >5 m wave heights [25-28]. Such storms usually have capability of eroding and transporting large boulders onshore upto a limited extent [5, 9, 19, 37, 38]. Based on the nature of storm deposits, their most specific characteristics can be studied during a post-event survey, however, those are not usually preserved along such a dynamic coast. Therefore, as the time passes their discrimination from tsunami deposits becomes more difficult.

Table 1 Calculation of wave velocity and wave height in case of storm and tsunami events by using the boulder parameters i.e., length (a-axis), width (b-axis) and height (c-axis), and components of the forces applied during the time when a wave hits a submerged or sub-aerially exposed boulder (Using Nott's modified mathematical approach). (V, H_s) and (V, H_r) domains represent the required wave velocity and wave height to transport such boulders respectively in case of a storm and a tsunami event [1, 18].

Boulders	a - Axis (m)	b - Axis (m)	c - Axis (m)	Volume (m ³)	Density (Kg/m ³)	Mass (Kg) M _{bl} = ρ.abc	Weight (KN) F _G = mg	Wave Velocity (v) (m/s)	Wave Height (H _r) (m)	Wave Height (H _s) (m)
B-1	1.54	1.1	0.3	0.51	2.70 x 10 ³	1.37 x 10 ³	1.35 x 10 ⁴	6.32	1.02	4.07
B-2	1.65	0.8	0.36	0.48	2.70 x 10 ³	1.28 x 10 ³	1.26 x 10 ⁴	5.32	0.72	2.89
B-3	1.3	0.95	0.35	0.43	2.70 x 10 ³	1.17 x 10 ³	1.14 x 10 ⁴	5.92	0.89	3.58
B-4	1.35	0.75	0.4	0.41	2.70 x 10 ³	1.09 x 10 ³	1.07 x 10 ⁴	4.98	0.63	2.53
B-5	2.9	1.68	0.5	2.44	2.70 x 10 ³	6.58 x 10 ³	6.45 x 10 ⁴	7.87	1.58	6.31
B-6	2.62	1.98	0.48	2.49	2.70 x 10 ³	6.72 x 10 ³	6.60 x 10 ⁴	8.35	1.78	7.11
B-7	1.98	1.76	0.41	1.43	2.70 x 10 ³	3.86 x 10 ³	3.78 x 10 ⁴	7.82	1.56	6.24
B-8	2.36	1.86	0.38	1.67	2.70 x 10 ³	4.50 x 10 ³	4.42 x 10 ⁴	7.83	1.56	6.24
B-9	2.18	1.65	0.36	1.29	2.70 x 10 ³	3.50 x 10 ³	3.43 x 10 ⁴	7.48	1.43	5.70
B-10	2.46	1.88	0.48	2.22	2.70 x 10 ³	5.99 x 10 ³	5.88 x 10 ⁴	8.20	1.71	6.86
B-11	1.92	1.64	0.41	1.29	2.70 x 10 ³	3.49 x 10 ³	3.42 x 10 ⁴	7.64	1.49	5.94
B-12	2.08	1.67	0.45	1.56	2.70 x 10 ³	4.22 x 10 ³	4.14 x 10 ⁴	7.78	1.54	6.17
B-13	2.25	1.89	0.46	1.96	2.70 x 10 ³	5.28 x 10 ³	5.18 x 10 ⁴	8.16	1.70	6.80
B-14	2.15	1.76	0.44	1.66	2.70 x 10 ³	4.50 x 10 ³	4.41 x 10 ⁴	7.91	1.59	6.38
B-15	1.94	1.65	0.39	1.25	2.70 x 10 ³	3.37 x 10 ³	3.31 x 10 ⁴	7.59	1.47	5.88

Table 2 Under Joint-bound boulder pre-setting, calculation of wave velocity and wave height in case of storm and tsunami events by using the boulder parameters, i.e., length (a-axis), width (b-axis) and height (c-axis), and components of the forces applied during the time when a wave hits a submerged or sub-aerially exposed and jointed boulders (Using Nott's modified mathematical approach) [1, 18].

Boulders	a - Axis (m)	b - Axis (m)	c - Axis (m)	Volume (m ³)	Density (Kg/m ³)	Mass (Kg) M _{bl} = ρ.abc	Weight (KN) F _G = mg	Wave Velocity (v) (m/s)	Wave Height (H _r) (m)	Wave Height (H _s) (m)
B-1	1.54	1.1	0.3	0.51	2.70 x 10 ³	1.37 x 10 ³	1.35 x 10 ⁴	6.32	1.70	6.80
B-2	1.65	0.8	0.36	0.48	2.70 x 10 ³	1.28 x 10 ³	1.26 x 10 ⁴	5.32	2.04	8.16
B-3	1.3	0.95	0.35	0.43	2.70 x 10 ³	1.17 x 10 ³	1.14 x 10 ⁴	5.92	1.98	7.93
B-4	1.35	0.75	0.4	0.41	2.70 x 10 ³	1.09 x 10 ³	1.07 x 10 ⁴	4.98	2.27	9.07
B-5	2.9	1.68	0.5	2.44	2.70 x 10 ³	6.58 x 10 ³	6.45 x 10 ⁴	7.87	2.61	11.06
B-6	2.62	1.98	0.48	2.49	2.70 x 10 ³	6.72 x 10 ³	6.60 x 10 ⁴	8.35	2.72	11.88
B-7	1.98	1.76	0.41	1.43	2.70 x 10 ³	3.86 x 10 ³	3.78 x 10 ⁴	7.82	2.32	9.29
B-8	2.36	1.86	0.38	1.67	2.70 x 10 ³	4.50 x 10 ³	4.42 x 10 ⁴	7.83	2.15	8.61
B-9	2.18	1.65	0.36	1.29	2.70 x 10 ³	3.50 x 10 ³	3.43 x 10 ⁴	7.48	2.04	8.16
B-10	2.46	1.88	0.48	2.22	2.70 x 10 ³	5.99 x 10 ³	5.88 x 10 ⁴	8.20	2.31	9.98
B-11	1.92	1.64	0.41	1.29	2.70 x 10 ³	3.49 x 10 ³	3.42 x 10 ⁴	7.64	2.32	9.29
B-12	2.08	1.67	0.45	1.56	2.70 x 10 ³	4.22 x 10 ³	4.14 x 10 ⁴	7.78	2.55	10.20
B-13	2.25	1.89	0.46	1.96	2.70 x 10 ³	5.28 x 10 ³	5.18 x 10 ⁴	8.16	2.61	10.43
B-14	2.15	1.76	0.44	1.66	2.70 x 10 ³	4.50 x 10 ³	4.41 x 10 ⁴	7.91	2.49	9.97
B-15	1.94	1.65	0.39	1.25	2.70 x 10 ³	3.37 x 10 ³	3.31 x 10 ⁴	7.59	2.21	8.84

Though in this region the boulders deposits are restricted to 20-25m wide fringing zone from the shoreline, we cannot rule out a tsunami origin, as this localization may be subjected to the geomorphic barrier in the form of ≈8m high eolian dune and cliff. In this scenario, the speed of a tsunami or storm flow is dissipated by the eolian dune/cliff and the boulders are only transported upto rocky tract/beach ridge or dune/cliff base.

Further, these boulder deposits can also be correlated with the documented 1945 tsunamigenic earthquake of Makran subduction zone, where the parameters calculated in this study are fairly in agreement with the approximated minimum wave or flow energy of the tsunami hitting the Saurashtra coast. The 1945 was the deadliest event killing more than 4000 people by its earthquake and tsunami [40]. Based on simulation models and documented records, the 1945 tsunami waves reached a height of about 11–11.5m in the Gulf of Kutch and Saurashtra coast [12, 22, 40], which is much more than the calculated 'required wave height'.

The identification of tsunami and storm deposits in the stratigraphic horizons is comparatively easy as they are usually preserved in the topographic depressions, channels, swales, marshes, and back-dune environments [19, 31-34, 37]. However, the regions where boulders are the only available clasts, their discrimination from a storm origin is difficult. Imbrications have been observed in tsunami as well storm originated boulder deposits, however, tsunami involves longer transportation and erosion therefore features more roundness in boulders [5, 9, 19, 31-38].

In our study region, the shape and size of the boulders are of mixed nature, i.e., angular to rounded, small to large, and tetrahedral to polyhedral. The sedimentological records of the finer fractions (i.e., sand, silt, clay, microfossils) are not preserved nearshore due to dynamic nature of the coast [41] and therefore, the major discriminative features are not available to identify the type of events. However, it is confirmed from the documented records of tsunamis and storms in this region that both events possess the wave parameters required for transporting such boulders onshore. We postulate that the boulder aggregates of the eastern flank are the sequel outcome of 1945 and similar paleotsunamis as well as 1998 and similar cyclonic storms impacted along the Saurashtra coast.

Acknowledgement

The research was conducted with the funding and support of Indian Institute of Technology Kanpur and it is a result of a few field surveys along the Saurashtra coast. The authors fully acknowledged all the supporting agencies involved in the accomplishment of the research work.

References

- [1] Benner, R., Browne, T., Brückner, H., Kelletat, D., Scheffers, A. 2010. Boulder Transport by Waves: Progress in Physical Modeling, *Zeitschrift für Geomorphologie*, 54 (Suppl. 3): 127-146. DOI : <https://doi.org/10.1127/0372-8854/2010/0054S3-0022>
- [2] Browne, A. 2011. "Coarse coastal deposits as palaeo-environmental archives for storms and tsunamis", *PhD Thesis, Southern Cross University, ePublications@SCU*.
- [3] Bilham, R., Lodi, S., Hough, S., Bukhary, S., Khan, A.M., Rafeeqi, S.F.A. 2007. Seismic hazard in Karachi, Pakistan: uncertain past, uncertain future, *Seismological Research Letters*, 78(6): 601-613. DOI: <https://doi.org/10.1785/gssrl.78.6.601>
- [4] Byrne, D.E., Sykes, L.R., Davis, D.M. 1992. Great thrust earthquakes and aseismic slip along the plate boundary of the Makran subduction zone, *Journal of Geophysical Research*, 97: 449-478. DOI: <https://doi.org/10.1029/91JB02165>
- [5] Cox, R., O'boyle, L., Cytrynbaum, J. 2019. Imbricated Coastal Boulder Deposits Formed by Storm Waves, and Preserve a Long-Term Storminess Record, *Scientific Reports*, 9, 10784. DOI: <https://doi.org/10.1038/s41598-019-47254-w>
- [6] Nandasena, N.A.K., Paris, R., Tanaka, N. 2011. Reassessment of hydrodynamic equations: minimum flow velocity to initiate boulder transport by high energy events (storms, tsunamis), *Marine Geology*, 281(1-4): 70-84. DOI: <https://doi.org/10.1016/j.margeo.2011.02.005>
- [7] Goto, K., Chavanich, S.A., Imamura, F., Kunthasap, P., Matsui, T., Minoura, K., Sugawara, D., Yanagisawa, H. 2007. Distribution, origin and transport process of boulders deposited by the 2004 Indian Ocean tsunami at Pakarang Cape, Thailand, *Sedimentary Geology*, 202 (4): 821-837. DOI: <https://doi.org/10.1016/j.sedgeo.2007.09.004>
- [8] Goto, K., Okada, K., Imamura, F. 2009. Characteristics and hydrodynamics of boulders transported by storm waves at Kudaka Island, Japan, *Marine Geology*, 262 (1-4): 14-24. DOI: <https://doi.org/10.1016/j.margeo.2009.03.001>
- [9] Goto, K., Miyagi, K., Kawamura, H., Imamura, F. 2010. "Discrimination of boulders deposited by tsunamis and storm waves at Ishigaki Island, Japan", *Marine Geology*, 269 (1-2): 34-45. DOI: <https://doi.org/10.1016/j.margeo.2009.12.004>
- [10] Heidarzadeh, M., Pirooz, M.D., Zaker, N.H., Yalciner, A.C., Mokhtari, M., Esmaeily, A. 2008. Historical tsunami in the Makran subduction zone off the southern coasts of Iran and Pakistan and results of numerical modeling, *Ocean Engineering*, 35: 774-786. DOI: <https://doi.org/10.1016/j.oceaneng.2008.01.017>
- [11] Heidarzadeh, M., Pirooz, M.D., Zaker, N.H., Yalciner, A.C., 2009. "Preliminary estimation of the tsunami hazards associated with the Makran subduction zone at the northwestern Indian Ocean", *Natural Hazards*, 48: 229-243. DOI: <https://doi.org/10.1007/s11069-008-9259-x>
- [12] Jaiswal, R.K., Singh, A.P., Rastogi, B.K., 2009. Simulation of the Arabian Sea tsunami propagation generated due to 1945 Makran earthquake and its effect on western parts of Gujarat (India), *Natural Hazards*, 48: 245-258. DOI: <https://doi.org/10.1007/s11069-008-9261-3>
- [13] Jordan, B.R. 2008. Tsunamis of the Arabian Peninsula - a guide of historic events", *Science of Tsunami Hazards*, 27: 31-46.
- [14] Imamura, F., Goto, K., Ohkubo, S. 2008. A numerical model for the transport of a boulder by tsunami, *Journal of Geophysical Research: Oceans*, 113(C1). DOI: <https://doi.org/10.1029/2007JC004170>
- [15] Nott, J. 1997. Extremely high energy wave deposits inside the Great Barrier Reef Australia; determining the cause - tropical cyclone or tsunami, *Marine Geology*, 14 1, 193-207. DOI: [https://doi.org/10.1016/S0025-3227\(97\)00063-7](https://doi.org/10.1016/S0025-3227(97)00063-7)
- [16] Nott, J. 2000. Records of prehistoric tsunamis from boulder deposits. Evidence from Australia, *Science of Tsunami Hazards*, 18(1): 1-14.
- [17] Nott, J. 2003. Waves, coastal boulder deposits and the importance of the pre-transport setting, *Earth and Planetary Science Letters*, 210 (1-2): 269-276. DOI: [https://doi.org/10.1016/S0012-821X\(03\)00104-3](https://doi.org/10.1016/S0012-821X(03)00104-3)
- [18] Nott, J. 2003. Tsunami or Storm Waves? - Determining the Origin of a Spectacular Field of Wave Emplaced Boulders Using Numerical Storm Surge and Wave Models and Hydrodynamic Transport Equations", *Journal of Coastal Research*, 19 (2): 348-356.
- [19] Mottershead, D.N., Soar, P.J., Bray, M.J., Hastewell, L.J. 2020. Reconstructing Boulder Deposition Histories: Extreme Wave Signatures on a Complex Rocky Shoreline of Malta, *Geosciences*, 10, 400. DOI: <https://doi.org/10.3390/geosciences10100400>
- [20] Shah-hosseini, M., Morhange, C., Naderi Beni, A., Marriner, N., Lahijani, H., Hamzeh, M., Sabatier, F. 2011. Coastal boulders as evidence for high-energy waves on the Iranian coast of Makran", *Marine Geology*, 290(1-4): 17-28. DOI: <https://doi.org/10.1016/j.margeo.2011.10.003>
- [21] Page, W.D., Alt, J.N., Cluff, L.S., Plafker, G. 1979. Evidence for the recurrence of large magnitude earthquakes along the Makran coast of Iran and Pakistan, *Developments in Geotectonics*, 13: 533-547. DOI: <https://doi.org/10.1016/B978-0-444-41783-1.50081-7>

- [22] Pararas-Carayannis, G. 2006. The potential of tsunami generation along the Makran subduction zone in the northern Arabian Sea – case study: the earthquake of November 28, 1945, *Science of Tsunami Hazard*, 24:358–384.
- [23] Regard, V., Bellier, O., Thomas, J.C., Boulès, D., Bonnet, S., Abbassi, M.R., Braucher, R., Mercier, J., Shabanian, E., Soleymani, S., Feghhi, K. 2005. Cumulative right-lateral fault slip rate across the Zagros–Makran transfer zone: role of the Minab–Zendan fault system in accommodating Arabia–Eurasia convergence in southeast Iran”, *Geophysical Journal International*, 162(1): 177-203. DOI: <https://doi.org/10.1111/j.1365-246X.2005.02558.x>
- [24] Okal, E.A., Synolakis, C.E. 2008. Far-field tsunami hazard from megathrust earthquakes in the Indian Ocean”, *Geophysical Journal International*, 172: 995-1015. DOI: <https://doi.org/10.1111/j.1365-246X.2007.03674.x>
- [25] Murty, T.S., El-Sabh, M.I. 1984. Cyclones and storm surges in the Arabian Sea: A brief review, *Oceanographic Research Papers*, 31: 665-670. DOI: [https://doi.org/10.1016/0198-0149\(84\)90034-7](https://doi.org/10.1016/0198-0149(84)90034-7)
- [26] Evan, A.T., Camargo, S.J. 2011. A climatology of Arabian Sea cyclonic storms”, *Journal of Climate*, 24(1), pp.140-158. DOI : <https://doi.org/10.1175/2010JCLI3611.1>
- [27] Dibajnia, M., Soltanpour, M., Nairn, R., Allahyar, M. 2010. Cyclone Gonu: The Most Intense Tropical Cyclone on Record in the Arabian Sea, In: Charabi Y (Ed.), *Indian Ocean tropical cyclones and climate change*, Springer Netherlands, pp. 149-157. DOI: https://doi.org/10.1007/978-90-481-3109-9_19
- [28] Fritz, H.M., Blount, C., Albusaidi, F.B., Al-Harthy, A.H.M. 2010. Cyclone Gonu Storm Surge in the Gulf of Oman, In: Charabi, Y. (Ed.), *Indian Ocean tropical cyclones and climate change*, Springer Netherlands, pp. 255-263. DOI: https://doi.org/10.1007/978-90-481-3109-9_30
- [29] Kopp, C., Fruehn, J., Flueh, E.R., Reichert, C., Kukowski, N., Bialas, J., Klaeschen, D. 2000. Structure of the Makran subduction zone from wide-angle and reflection seismic data, *Tectonophysics*, 329(1-4): 171-191. DOI: [https://doi.org/10.1016/S0040-1951\(00\)00195-5](https://doi.org/10.1016/S0040-1951(00)00195-5)
- [30] Rajendran, C.P., Ramanamurthy, M.V., Reddy, N.T., Rajendran, K. 2008. Hazard implication of the late arrival of the 1945 Makran tsunami, *Current Science, India* 95: 1739-1743.
- [31] Noormets, R., Crook, K., Felton, E. 2004. Sedimentology of rocky shorelines: 3.: Hydrodynamics of megaclast emplacement and transport on a shore platform, Oahu, Hawaii, *Sedimentary Geology*, 172: 41 – 65. DOI: [https://doi.org/10.1016/S0037-0738\(04\)00235-0](https://doi.org/10.1016/S0037-0738(04)00235-0)
- [32] Malik, J.N., Shishikura, M., Echigo, T., Ikeda, Y., Satake, K., Kayanne, H., Sawai, Y., Murty, C.V.R., Dikshit, O. 2011. Geologic evidence for two pre-2004 earthquakes during recent centuries near Port Blair, South Andaman Island, India, *Geology*, 39(6): 559-562. DOI: <https://doi.org/10.1130/G31707.1>
- [33] Malik, J.N., Banerjee, C., Khan, A., Johnson, F.C., Shishikura, M., Satake, K., Singhvi, A.K. 2015. Stratigraphic evidence for earthquakes and tsunamis on the west coast of South Andaman Island, India during the past 1000 years, *Tectonophysics*, 661: 49-65. DOI: <https://doi.org/10.1016/j.tecto.2015.07.038>
- [34] Malik, J.N., Johnson, F.C., Khan, A., Sahoo, S., Irshad, R., Paul, D., Arora, S., Baghel, P.K., Chopra, S. 2019. Tsunami records of the last 8000 years in the Andaman Island, India, from mega and large earthquakes: Insights on recurrence interval, *Scientific Reports*, 9(1): 1-14. DOI: <https://doi.org/10.1038/s41598-019-54750-6>
- [35] Mastronuzzi, G., Sansò, P. 2004. Large boulder accumulations by extreme waves along the Adriatic Coast of southern Apulia (Italy), *Quaternary International*, 120, 173–184. DOI: <https://doi.org/10.1016/j.quaint.2004.01.016>
- [36] Switzer, A.D., Burston, J.M. 2010. Competing mechanisms for boulder deposition on the southeast Australian coast”, *Geomorphology*, 114 (1-2): 42-54. DOI: <https://doi.org/10.1016/j.geomorph.2009.02.009>
- [37] Tuttle, M.P., Ruffman, A., Anderson, T., Jeter, H. 2004. Distinguishing tsunami from storm deposits in eastern North America: The 1929 Grand Banks tsunami versus the 1991 Halloween storm, *Seismological Research Letters*, 75, 117–131. DOI: <https://doi.org/10.1785/gssrl.75.1.117>
- [38] Williams, D.M., Hall, A.M. 2004. Cliff-top megaclast deposits of Ireland, a record of extreme waves in the North Atlantic—storms or tsunamis? *Marine Geology*, 206:101–117. DOI: <https://doi.org/10.1016/j.margeo.2004.02.002>
- [39] Ambraseys, N.N., C.P. Melville. 1982. A history of Persian earthquakes, Cambridge (NY): Cambridge University Press. URL: <https://catalogue.nla.gov.au/Record/133972>
- [40] Pendse, C.G. 1946. The Mekran earthquake of the 28th November 1945”, Scientific Notes, *Indian Meteorological Department*, 10:141145.
- [41] Johnson, F.C., Malik, J.N., Kathal, P.K., Khan, A. 2021. Foraminiferal Assemblages of Inferred Onshore Paleotsunami Deposits in Southwestern Andaman Islands, India. *Journal of the Geological Society of India*, 97(6): 579–595. DOI: <https://doi.org/10.1007/S12594-021-1733-Z>